Progress In Electromagnetics Research C, Vol. 91, 69–82, 2019

A Novel Lightweight SARNet with Clock-Wise Data Amplification for SAR ATR

Yikui Zhai[1], Wenbo Deng[1], Yanqing Zhu[2], Ying Xu[1, *], Bing Sun[2], Jingwen Li[2], Qirui Ke[1], Yihang Zhi[1], and Vincenzo Pirui[3]

Abstract—Convolutional Neural Network (CNN) models applied to synthetic aperture radar automatic target recognition (SAR ATR) universally focus on two important issues: overfitting caused by lack of sufficient training data and independent variations like worse estimates of the aspect angle, etc. To this end, we developed a lightweight CNN-based method named SARNet to accomplish the classification task. Firstly, a clock-wise data amplification approach is presented to generate adequate SAR images without requiring many raw SAR images, effectively avoiding overfitting in the course of training. Then a SARNet is devised to process the extracted features from SAR target images and work on classification tasks with parameters fine-tuning under comparative models. To enhance and structurally organize the representation of learned proposed model, various activation functions are explored in this paper. Furthermore, due to the pioneering conducted experiments, training samples in the MSTAR and extended MSTAR database are utilized to demonstrate the robustness and effectiveness of the lightweight model. Experimental results have shown that our proposed model has achieved a 98.30% state-of-the-art accuracy.

1. INTRODUCTION

Target recognition in synthetic aperture radar (SAR) images has several promising applications in the various fields, such as enemy identification, battlefield surveillance, and disaster relief program. SAR technology could provide more information in multi-fields, such as topographic information for mineral exploration, prospection for oil spill boundaries, navigation for sea state and ice hazard maps, and reconnaissance for military operations [1, 2]. Therefore, SAR ATR has become one of the most challenging issues in its applications.

Traditionally, typical classification task relevant to SAR target images could be summarized as two processes: feature extraction and classification. Feature extraction techniques including principal component analysis (PCA) [3], linear discriminant analysis (LDA) [4], histogram of oriented gradients (HOG) feature extraction [5], and nonnegative matrix factorization (NMF) [6] have been proposed. PCA and LDA are two principal algorithms for dimensionality reduction in the classification task. The basic difference between them is that LDA uses information of classes to find features in order to maximize its separability while PCA uses the variance of each feature to do the same. HOG feature extraction returned the features that could encode local shape information from regions within an image. NMF is a widely used tool for the analysis of high-dimensional data as it automatically extracts sparse and meaningful features from a set of nonnegative data vectors. Then classification approaches such as support vector machine (SVM) [7], decision tree [8], and Bayesian classifier [9] have been presented as well. SVM is an algorithm used for classification problems similar to Logistic Regression (LR). The

Received 3 December 2018, Accepted 2 February 2019, Scheduled 20 March 2019
* Corresponding author: Ying Xu (xuying117@163.com).
[1] Department of Intelligent Manufacturing, Wuyi University, China. [2] School of Electronics and Information Engineering, Beihang University, Beijing, China. [3] Dipartimento di Informatica, Universita' Degli Studi di Milano, via Celoria 18, Milano (MI), Italy.

objective of the algorithm is to find the hyperplane that has the maximum margin in an N-dimensional space that distinctly classifies the data points. A decision tree is a decision support tool that uses a tree-like model of decisions and their possible consequences. Bayes is a simple widely used technique for constructing classifiers: models that assigned class labels to problem instances, represented as vectors of feature values, where the class labels were drawn from some finite set; however, artificial scenes and natural objects may suffer from large mirror reflections associated with microwave mirroring, speckle noise, and complex azimuth cases [10]. Additionally, the probability of correct classification decreases with worse estimates of the aspect angle and limited raw image data. All these factors will lead to more difficulties in SAR ATR.

In this paper, a lightweight SARNet model with clock-wise data amplification operation is proposed for SAR ATR. Firstly, clock-wise data amplification approach is utilized to generate sufficient training samples. Then a lightweight SARNet is designed to reduce the parameters produced from layer by layer. Several activation functions are also studied to validate the representation of the extracted features. The contributions of this paper are as follows:

(i) The aim of the presented clock-wise data amplification is to avoid overfitting and address the drawback that SAR image is prone to severe image rotation.

(ii) The architecture of proposed models is lightweight and simple; however, the accuracy is greatly improved compared with the method employed to traditional and complex network, much reducing the memory requirement and redundant computation.

(iii) Comprehensive experiments were performed to empirically explore the SARNet model with different parameters on the extended MSTAR database.

2. RELATED WORK

Traditional approaches applied into SAR ATR task have achieved promising results [11–25]. In 2001, Zhao and Principe [11] input original pixels from SAR target images to the support vector machine (SVM) classifier to form a local "bounded" decision region around each class that presents better rejection to confusers Sun et al. [12] extracted features of the magnitudes of the 2-D DFT coefficients from preprocessed images. In order to enhance the classification performance, Zhou et al. [13] identified scattering centers by physical correlation and predicted results from the global scattering center model. Park et al. [14] presented discriminative features on projection length and target pixels for discriminating targets from clutter in high-resolution synthetic aperture radar imagery. Dong et al. [15] provided an approach of the monogenic signal through sparse representation to code the feature vector of the test sample as a sparse linear combination of them. Carmine et al. [16] extracted pseudo-Zernike moments of multichannel images for SAR ATR. Mishra and Mulgrew [17] also studied principal component analysis (PCA) method to reduce the dimension for less computation with parameters for SAR ATR Ash [18] used the local binary pattern (LBP) and other texture feature extraction methods to address the change detection for robust exploitation in interrupted SAR environments. Zhang et al. [19] adopted a new classifier for polarimetric SAR images to acquire robust features. Zhai et al. [20] proposed a multi-scale local phase quantization plus biometric pattern recognition to do with SAR target images. For addressing the changes of SAR target detection problem Misha and Susaki [21] presented a region algorithm based on change detection in SAR image. Gao et al. [22] modeled SAR images with generalized Gamma distribution for text component. At the same time. Cheng et al. [23] tried an improved scheme for parameter estimation of G° distribution model in high-resolution SAR images. Ni et al. [24] proposed a Matrix Analysis and Multi-threshold Segmentation algorithm to obtain the interested region of SAR target images. Fu [25] also proposed a SAR target recognition method based on target region matching. However, the above algorithms for feature extraction are often designed manually and not extracted in detail, resulting in time consumption and labor waste with unsatisfactory results.

In the past few decades, above traditional approaches and advanced CNN methods of image classification have advanced the understanding of tasks related to SAR target images. Inspired by the feature extraction and classification method in many traditional techniques. Ding et al. [26] tried to conduct image transformations on SAR images and managed to apply to the existing CNN models with comparative results. With the goal of optimizing the output parameters, Chen et al. [27] focused on the classification scheme selecting spectral-spatial features. Zhao and Du [28] proposed a spectral-spatial feature based classification (SSFC) algorithm by combining the dimension reduction block and deep learning techniques. Marmanis et al. [29] applied convolution neural network and deep learning algorithm on SAR ATR task, which served more in the field of SAR ATR [30–34]. Liu et al. [35] presented a SAR target image classification method with CNN based on transfer learning and reached comparable results. Convolution neural network obtains its advantage through end-to-end learning and can be trained by the standard back-propagation algorithm. All these suggest the promising potential of CNN-based in feature extraction and feature learning.

The organization of this paper can be summarized as follows. Section 3 introduces the proposed networks and details the extended MSTAR database. Section 4 presents the experimental results on public databases. Finally, conclusions are presented in Section 5.

3. PROPOSED METHOD

In this section, we propose a lightweight SARNet model for SAR ATR, to accomplish the SAR images classification task effectively with data amplification. Firstly, we will illustrate the structure, implementation, and characteristics of the proposed network. Then the ROI extraction and clock-wise data amplification are detailed. Finally, a few derivations will be given under mythology architecture.

3.1. Proposed Network

To the best of our knowledge, it is supposed that an amount of time will be taken to reduce the parameters of a large-scale network in the SAR ATR assignment. In this paper, a two-layer convolution layer neural network is designed. The diagram of SARNet presented is illustrated in Figure 1.

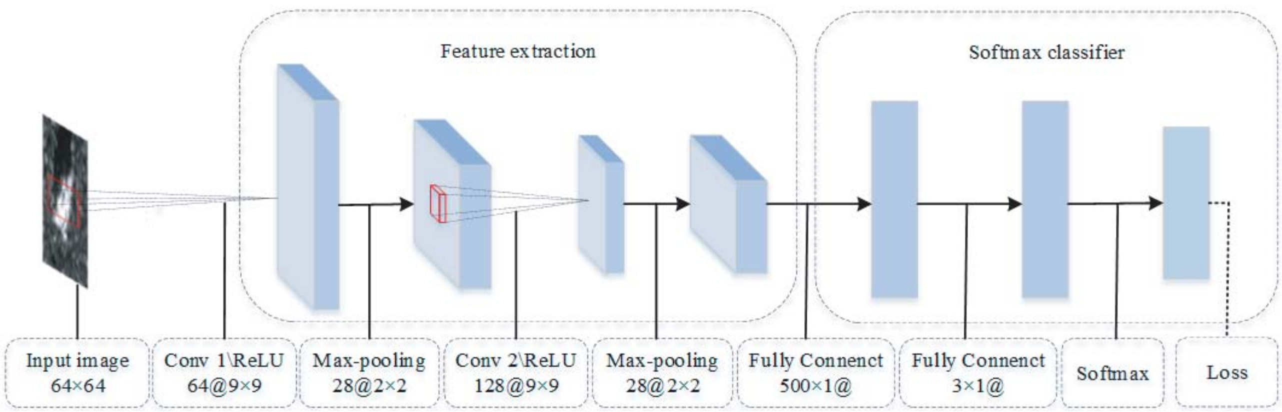

Figure 1. The diagram of the proposed network.

The network model consists of two layers of basic layer convolution 1 (Conv1) and convolution 2 (Conv2). The layer Conv1 outputs 64 feature maps, and Conv2 outputs 128 feature maps with two layers. The pool layers pooling1 (P1) and pooling2 (P2) both adopt the maximum pool. F1 and F2 are the fully connected layers. F1 outputs 500 neurons, and F2 outputs 3 neurons. After F2 convolution layer, softmax classifier is used to output the classification results. In the network, ReLU activation is employed in this paper to reduce the interdependence of parameters and alleviate the problem of over-fitting. The procedure of the network can be illustrated as Equation (1).

$$l(x, y, \theta) = \sum_{i=1}^{L} soft\max(W \cdot f(X_i; \theta), y_i) \tag{1}$$

where $x = \{X_i\}_{i=1}^{L}, y = \{y_i\}_{i=1}^{L}$; x, y are the input and output collections of the proposed network respectively; θ is the fine-tuned weights or the learned weights from training samples. W is the weight of input images, and L denotes the class number of the SAR target. $f(\cdot)$ means the features extracted from the previous layers. Softmax is a common classifier used in deep learning.

In the proposed classification pipeline, notice that parameters settings greatly affect the effectiveness of our network. Therefore, we maintain the variables such as iteration and batch size as fixed values to yield the best state of the network for SAR target images classification. The parameters of the proposed model are shown as Table 1.

Table 1. The proposed SARNet parameters setting.

Layer type	Output size	filter size/stride	depth	parameter
Input	$64 \times 64 \times 1$	-	-	-
Conv1	$56 \times 56 \times 64$	$9 \times 9/1$	1	5,248
Maxpool1	28×28	$2 \times 2/2$	0	-
Conv2	$20 \times 20 \times 128$	$9 \times 9/1$	1	663,680
Maxpool2	10×10	$2 \times 2/2$	1	-
Fc1	500	-	0	6,400,500
Fc2	3	-	0	1,503

3.2. ROI Extraction

Owing to the imaging characteristics of the aperture radar, background noise, especially speckle noise, generally exists in acquired training samples, considerably increasing the time of image processing and reducing the precision of classification task. Consequently, the region of interest (ROI) needs to b extracted from the original samples. Supposing that the radius of ROI is r, the function satisfies the following constrains under such a sense.

$$f(r, \varphi) = 0, (r, \varphi) \notin p^2 \tag{2}$$

where $f(\cdot)$ is a set of points satisfying $f(\cdot) = 0$ by substituting all the point coordinates without the centroid of the images. φ is the included angle with level line.

As expected, there would be some blank area in the images after clock-wise data amplification to degrade the classification performance. The idea is to reconstruct the area as a circle which is not prone to the operation. The region of reconstruction is defined as

$$Loc(x, y) = \left\{(x, y)|(x - x_0)^2 + (y - y_0)^2 = r^2\right\} \tag{3}$$

In general, when a part of the area of interest is reconstructed, a small amount of adjacent information outside the area being considered is added for reconstruction as raw data. In order to obtain ROI image from original image, we locate the centroid of each image to resize the region from the reconstructed area. Based on the centroid (x_0, y_0), the scale of the length is from $x_0 - l/4$ to $x_0 + l/4$. The height is from $y_0 - l/4$ to $y_0 + l/4$ where l and h are the length and height of the raw image. SAR images are illustrated in Figure 2. Figure 2(a) describes the original images, and Figure 2(b) shows the ROI. The resized SAR images share the size of $l = 64$, $h = 64$.

3.3. Clock-Wise Data Amplification

For SAR image, the aspect angle of the target is primarily prone to the imaging results, while the azimuth and angle of the image are not generally complete, greatly producing negative effect of SAR ATR. The strategy is to change the aspect angel to extend the dataset on the basis that the pitch angle of SAR image is not sensitive to the change, and the method that rotates the SAR target images degrees by degrees is named clock-wise data amplification to generate sufficient training samples, addressing the challenging problem of overfitting and sample shortages.

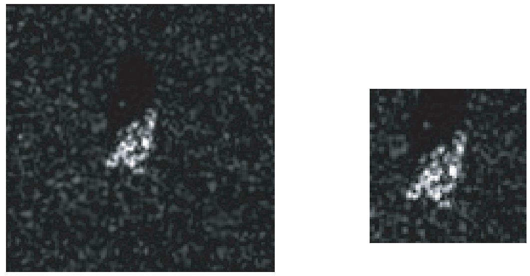

(a) (b)

Figure 2. Raw SAR image and ROI image. (a) Raw image. (b) ROI image.

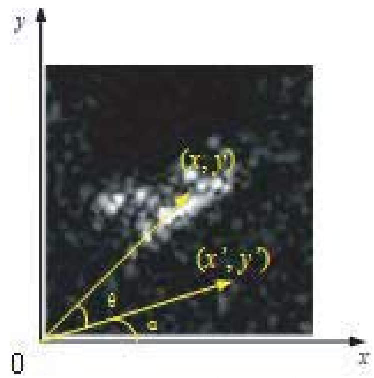

Figure 3. Image transformation process.

As shown in Figure 3, $(x,\, y)$ is the location of the image pixel, and $(x',\, y')$ is the associated location after transformation. The transformation formula is as follows:

$$\begin{cases} \tan(\theta+\alpha) = \dfrac{y'}{x'} \\ \tan\alpha = \frac{y}{x} \\ x^2 + y^2 = x'^2 + y'^2 \end{cases} \tag{4}$$

By means of mathematical transformations, the equation can be simplified as equality in Eq. (5).

$$\begin{cases} x' = x\cos\theta + y(-\sin\theta) \\ y' = x\sin\theta + y\cos\theta \end{cases} \tag{5}$$

Note that affine transformation matrices can be represented as:

$$A = \begin{bmatrix} \cos\theta & -\sin\theta \\ \sin\theta & \cos\theta \end{bmatrix} \tag{6}$$

To avoid the deficiency of information in SAR target images, a shift will be added as:

$$\begin{aligned} x' &= (x - x_0)\cos\theta + (y - y_0)(-\sin\theta) + x_0 + \Delta x \\ y' &= (x - x_0)\sin\theta + (y - y_0)(\cos\theta) + y_0 + \Delta y \end{aligned} \tag{7}$$

By using the backward mapping in the image, the annotations of x', $y'x'$, y' can be interpret as x, yx, y, then such a formula is changed into the equation as:

$$\begin{aligned} x &= ((x' - x_0 - \Delta x)\cos\theta + (y' - y_0 - \Delta y)(\sin\theta)/scale + x_0 \\ y &= ((x - x_0 - \Delta x)(-\sin\theta) + (y' - y_0 - \Delta y)(\cos\theta)/scale + y_0 \end{aligned} \tag{8}$$

For the MSTAR database, training samples are under the process of clock-wise data amplification. The extended database is 360 times of the amount of data compared to the original MSTAR database. ROI Images with different degree clock-wise data amplification are shown in Figure 4.

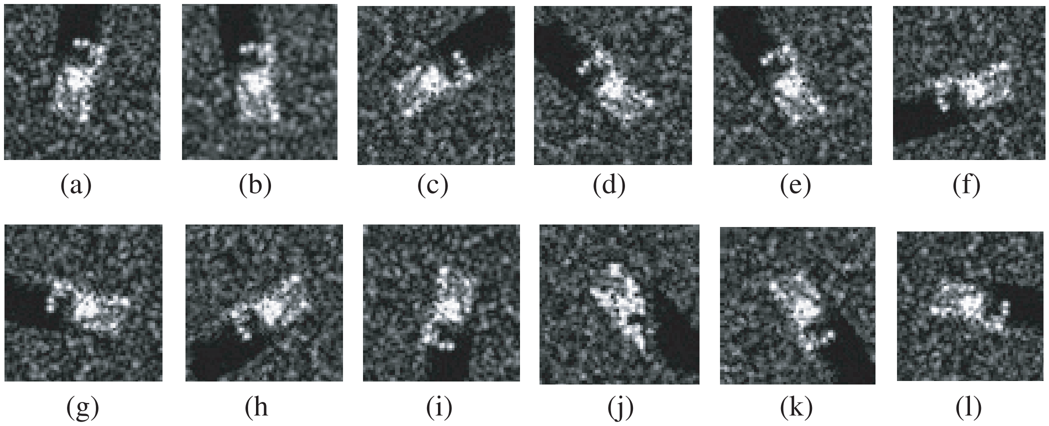

Figure 4. ROI Images with different degree clock-wise data amplification.

4. EXPERIMENTAL RESULTS AND ANALYSIS

In this paper, the experiments are conducted on acceleration computing service with Intel Core i3-7350K CPU, on Ubuntu 16.04 LTS operation system. NVIDIA GTX 1080ti is selected to process the images, and the capability of RAM is 8G. The proposed convolutional neural network model is implemented using the publicly available Caffe framework.

4.1. MSTAR Database

4.1.1. Original Database

With the objective of exploiting the performance on SAR target images classification task, the MSTAR SAR dataset was performed to test the model. The dataset was derived from the MSTAR project with three categories.The configuration of the MSTAR three-target database is shown in Table 2. The training and testing sets released in public are the target image with different aspects and depression angles. The training and testing samples, acquired from T72_SN132 (Main Battle Tanks), BMP2_SNC21 (Armored Personal Carriers), BTR70_SCN71 (Armored Personal Carriers), are utilized for the experiments presented in this paper. The total dataset for the work had 698 images incorporating 232 BMP2_SNC21, 233 BTR70_SCN71, and 233 T72_SN132 images. For the entire training dataset, we randomly select 75% for training and 25% for validation. The optical images are illustrated in Figure 5, and SAR images are illustrated in Figure 6.

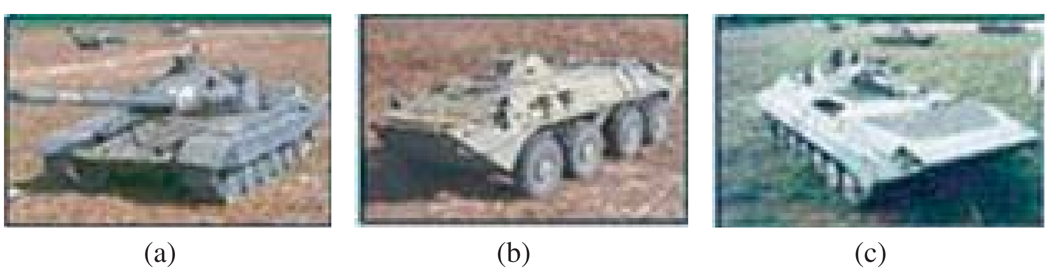

Figure 5. Optical images of three kinds of targets. (a) T72_SN132. (b) BTR70_SCN71. (c) BMP2_SNC21.

4.1.2. Extended MSTAR DATASET

The MSTAR database contains 698 raw SAR images with three categories. The mumble is 232, 233, and 233, respectively. The extended MSTAR dataset through clock-wise data amplification incorporates

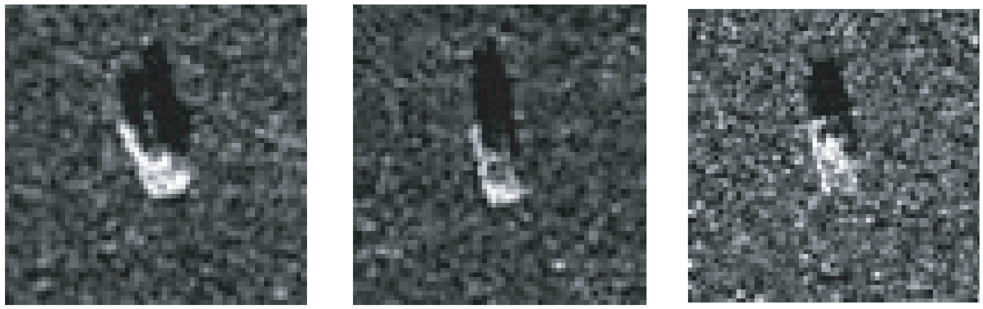

(a) (b) (c)

Figure 6. SAR Imaging of three kinds of targets. (a) T72_SN132. (b) T72_SN132. (c) BMP2_SNC21.

Table 2. The configuration of the MSTAR three-target database.

Training Set	Number	Testing Set	Number
T72_SN132	232	T72_SN132	196
T72_SN812	231	T72_SN812	195
T72_SNS7	228	T72_SNS7	191
BMP2_SNC21	233	BMP2_SN9563	195
BMP2_SN9566	232	BMP2_SN9566	196
BMP2_SNC21	233	BMP2_SNC21	196
BTR70_SNC71	233	BTR70_SNC71	196

254770 images, and the capability is summed up to 1.01G. The image size is 64×64 pixels with grayscale image type. Squash is selected as the resize transformation and IMDB as DB backend. There is no database compression in the testing database. For the original SAR datasets, 524 images are utilized to train the SARNet model, and 174 images are used as validation database. All experiments on an extended database include 254770 images, and 1365 images are employed as a validation database as well as testing database to validate the performance of presented models. Database distributions of the original and extended datasets are shown as in Figure 7.

4.2. Iteration of Training

In the course of training, 60 epochs are selected to fine-tune the models; meantime, information about the loss values and output classification results is recorded as well. As depicted in Figure 8, the accuracy has increased to a superior value in the earlier training stage and maintains a stable state afterwards.

The performance has attained a great improvement when fixing the epochs to 60. The phrase of training process is shown in Figure 8, and it has demonstrated the robustness and efficiency of the presented network, which received a faster convergence speed and kept a relatively stable state at the end.

4.3. Analysis of the Proposed SARNet

In this section, significant elements of SARNet are explored for the lightweight model. Different network models are reconstructed to validate the performance on SAR image databases. The accuracy of network feature extraction under different parameters is tested, and the influence of different parameters on the test results is discussed in detail from Table 3 to Table 6.

As shown in Table 3, the relatively large convolution kernel is advantageous to extract informative features from SAR images, and the model with the convolution kernel size of 9×9 achieved the best

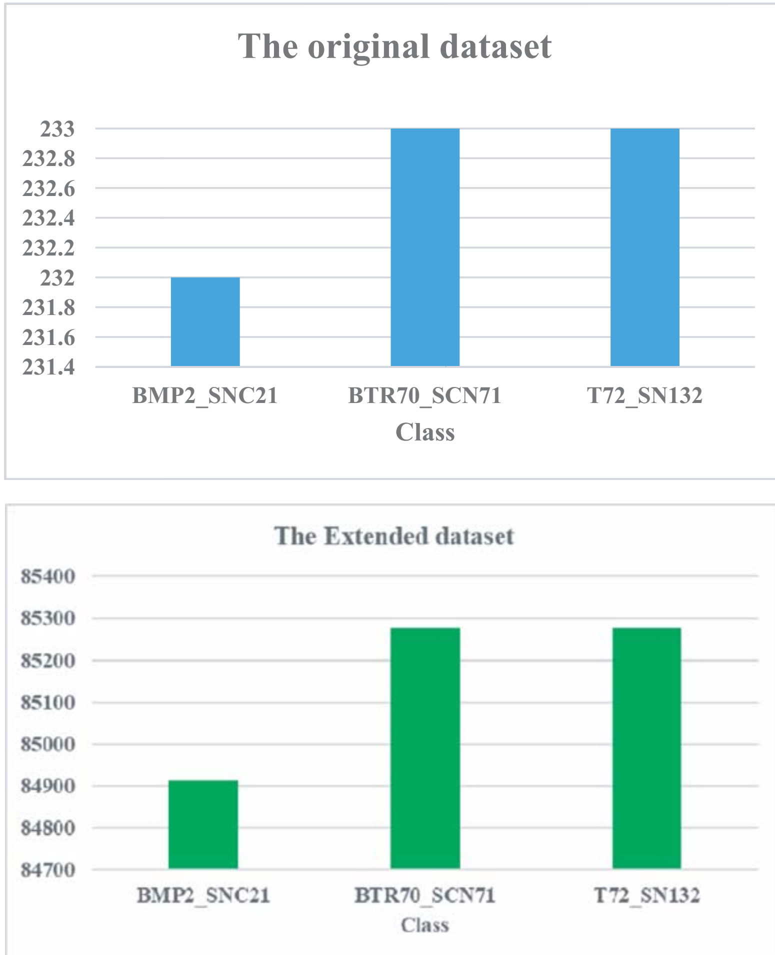

Figure 7. Database distributions of the original and extended datasets.

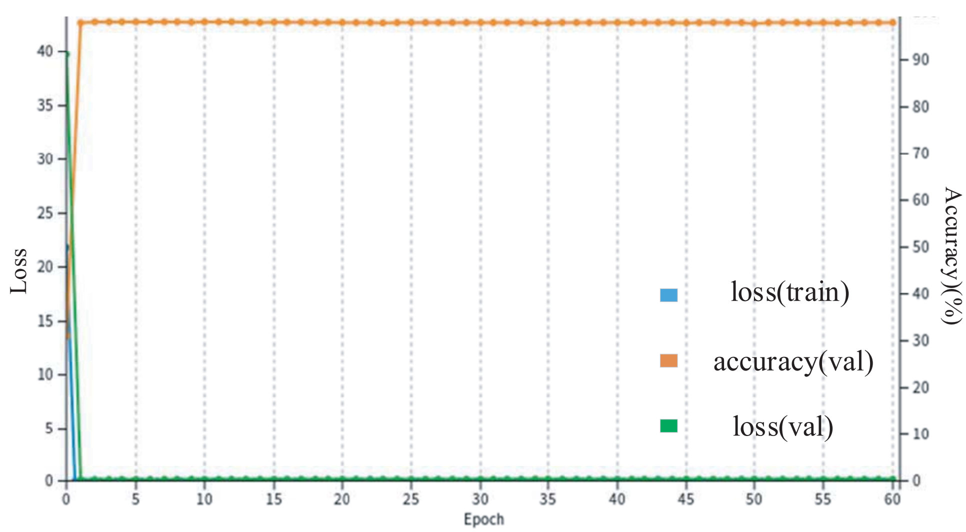

Figure 8. The phrase of training process.

Table 3. Effect of different convolution kernel sizes.

Net model	Conv1	Conv2	Fc	Accuracy
1	3/64	3/128	500	95.46%
2	5/64	5/128	500	95.38%
3	7/64	7/128	500	95.60%
4	9/64	9/128	500	95.75%
5	11/64	11/128	500	93.70%

Table 4. Effect of the number of layers.

Model	Conv1	Conv2	Conv3	Conv4	Fc	Accuracy
1	3/15	3/30	–	–	500	95.38%
2	3/15	3/30	3/60	–	500	95.53%
3	3/15	3/15	3/60	3/120	500	94.80%

Table 5. Effect of ReLU active function on the model.

Model	Conv-pooling1	ReLU	Conv-pooling2	ReLU	Accuracy
1	7/64, 2	Yes	7/128, 2	No	89.89%
2	7/64, 2	Yes	7/128, 2	Yes	95.60%

Table 6. Ablation study with variable activation functions.

Network	Activation	Accuracy
SARNet	Sigmoid	96.78%
	TanH	96.04%
	Power	42.64%
	ELU	97.36%
	ReLU	97.88%

effect. Table 4 demonstrates that two convolutional layers as the best parameters in terms of three convolutional layers considerably increase much complexity of the network. Table 5 indicates that activation function applied to the SARNet contributes to a satisfactory performance. Learned from Table 6, Ablation study on activation function demonstrates that the ReLU contributes to obtaining the best representation of the network and reaches better performance than other functions.

To get a deeper view and demonstrate the proposed network's capabilities, we visually examine different layers in Figure 9. In the proposed SARNet it shows that the learned filter size under several comparable experiments contributes to extracting more feature information, which contains informative information pertaining to the target. Observed from the visualization, it is not surprising that the proposed model could perform well in recognition.

4.4. Comparison Evaluation

4.4.1. Results on Original and Extended MSTAR Database

As indicated in Tables 7 and 8, it is apparent that data amplification helps in improving the performance of classification. The result of training sample without data amplification reaches 83.66%, lower than the result about 14.22% with clock-wise data amplification.

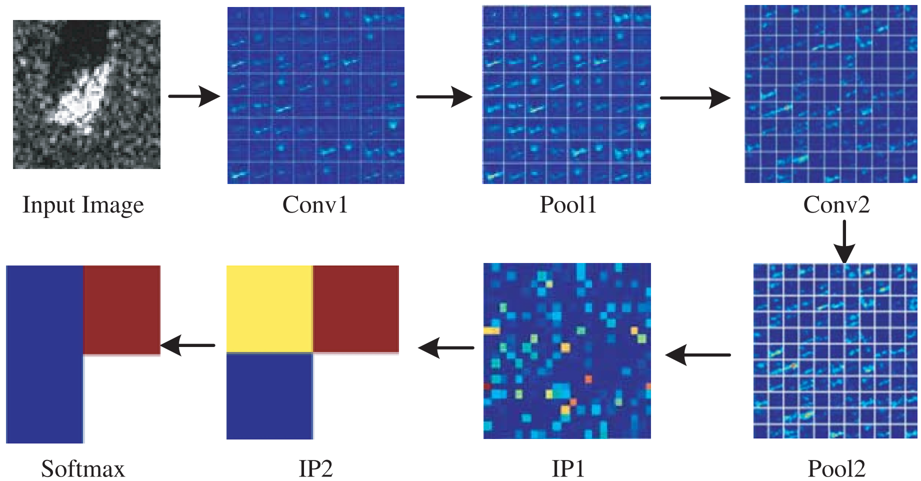

Figure 9. Visualization of different layers.

Table 7. Results on original MSTAR database.

Testing Target	Result			Accuracy
	BMP2	BTR	T72	
BMP2	484	81	19	82.82%
BTR	71	471	45	80.24%
T72	1	6	189	96.43%
Overall Accuracy	83.66%			

Table 8. Results on extended MSTAR database.

Testing Target	Result			Accuracy
	BMP2	BTR	T72	
BMP2	575	4	3	98.80%
BTR	19	566	2	96.42%
T72	1	0	195	99.19%
Overall Accuracy	97.88%			

As indicated in Table 9, different intervals of clock-wise experiments are designed to explore the performance of the proposed model. It is shown that different intervals benefit the classification task, indicating the significance of the sufficient training samples in deep learning method. It should be noticed that clock-wise data amplification works well to improve the performance; however, the performance of $45°$ interval of clock-wise is better than $1°$. There might be more redundancy and noise in the images via $1°$ interval of clock-wise, and it remains to be proved.

4.4.2. Comparison Experiments Analysis

As suggested in Table 10, the model produced from our network shares the lightweight capability of 28.3 M compared with other traditional and advanced method. Experimental performance in Tables 10 and 11 also demonstrates that our proposed method is robust and effective. The method using both dictionary learning and sparse representation reaches the result of 92.20%. The accuracy in CNN [38] is about 95.90%. The results of unsupervised K-means with data amplification obtain accuracy of 96.67%. The accuracy of our proposed method is superior to all the approaches in Table 11.

Table 9. Network accuracy via different clock-wise data amplification.

Network	Interval clock-wise	Accuracy
SARNet	1°	97.88%
	45°	98.30%
	60°	96.77%
	90°	96.94%
	120°	97.45%

Table 10. Comparisons with other state-of-the-art CNN models.

Method	Parameters	Accuracy	Storage
Alex-Net [36]	20,157,123	93.55%	80.6 M
Le-Net [37]	4,252,573	97.29%	17 M
ResNet-50 [38]	859,299	97.66%	3.5 M
SARNet	7,070,931	98.30%	28.3 M

Table 11. Comparison with other methods.

Method	Accuracy
Dictionary learning+ sparse representation [39]	92.20%
SVM [40]	93.54%
AlexNet [36]	93.55%
Single-scale LPQ binding [41]	94.75%
Gabor+LPM+ELM [42]	94.80%
A combination of sparse presentations [43]	95.60%
CNN [44]	95.90%
Adaptive feature selection method [45]	96.12%
Unsupervised K-means +Data Amplification [46]	96.67%
Le-Net [37]	97.29%
ResNet-50 [38]	97.66%
SARNet	98.30%

Table 10 shows the performance of the previous advanced methods. The parameters produced from SARNet are about 7,070,931, ranking the third listed in the table, while it reaches the best accuracy about 98.30%, even though the storage about SARNet is 28.3 M. In terms of overall performance, it has comparable advantages over state-of-the-art CNN model.

5. CONCLUSION

In this paper, a lightweight SARNet is presented to solve the challenging problems existing in SAR target images recognitions task. Firstly, ROI extraction and clock-wise data amplification are utilized to solve the drawback of limited original images, addressing the limitation of insufficient raw training samples. Then the learned parameters from comparative experiments are adapted to suit new lightweight SARNet models. Furthermore, the proposed SARNet has improved the effectiveness compared to state-of-the-art models on supervised classification and has strong robustness in the terms of the visual quality and classification accuracy. How to choose different intervals of clock-wise data amplification to benefit the performance of SAR ATR is a promising and valuable focus in the future work.

ACKNOWLEDGMENT

This work is supported by the National Natural Science Foundation of China (Grant No. 61771347), Characteristic Innovation Project of Guangdong Province (No. 2017KTSCX181), Youth Innovation Talent Project of Guangdong Province (No. 2016KQNCX171).

REFERENCES

1. Liu, S., M. Liu, P. Li, et al., "SAR image denoising via sparse representation in shearlet domain based on continuous cycle spinning," *IEEE TRGS*, Vol. 55, No. 5, 2985–2992, 2017.
2. Cloude, S. R. and E. Pottier, "An entropy based classification scheme for land applications of polarimetric SAR," *IEEE TRGS*, Vol. 35, No. 1, 68–78, 1997.
3. Singh, M. and G. Kaur, "SAR image classification using PCA and texture analysis," *Information Technology and Mobile Communication*, 435–439, Springer, Berlin, Heidelberg, 2011.
4. Mishra, A. K., "Validation of PCA and LDA for SAR ATR," *TENCON 2008 — 2008 IEEE Region 10 Conference*, 1–6, 2008.
5. Li, Q., G. Qu, and Z. Li, "Matching between SAR images and optical images based on HOG descriptor," *International Radar Conference IET*, 1–4, 2013.
6. Huan, R. H., Y. Pan, and K. J. Mao, "SAR image target recognition based on NMF feature extraction and Bayesian decision fusion," *IITA-GRS*, 496–499, 2010.
7. Cao, Z. J., Y. C. Ge, and J. L. Feng, "SAR image classification with a sample reusable domain adaptation algorithm based on SVM classifier," *Pattern Recognition*, 2017.
8. Khosravi, I., A. Safari, S. Homayouni, et al., "Enhanced decision tree ensembles for land-cover mapping from fully polarimetric SAR data," *IJRS*, Vol. 38, No. 23, 7138–7160, 2017.
9. Xu, G., M. Xing, L. Zhang, et al., "Bayesian inverse synthetic aperture radar imaging," *IEEE GRSL*, Vol. 8, No. 6, 1150–1154, 2011.
10. Huo, W., Y. Huang, J. Pei, et al., "Virtual SAR target image generation and similarity," *2016 IEEE International Geoscience and Remote Sensing Symposium (IGARSS)*, 914–917, IEEE, 2016.
11. Zhao, Q. and J. C. Principe, "Support vector machine for SAR automatic target recognition," *IEEE TGRS*, Vol. 37, No. 2, 643–654, 2001.
12. Sun, Y., Z. Liu, and J. Li, "Adaptive boosting for SAR automatic target recognition," *IEEE TGRS*, Vol. 43, No. 1, 112–125, 2007.
13. Zhou, J. X., Z. G. Shi, X. Cheng, and Q. Fu, "Automatic target recognition of SAR images based on global scattering center model," *IEEE TGRS*, Vol. 49, No. 10, 3713–3729, 2011.
14. Park, J., S. H. Park, and K. T. Kim, "New discrimination features for SAR automatic target recognition," *IEEE GRSL*, Vol. 10, No. 3, 476–480, 2013.
15. Dong, G., N. Wang, and G. Kuang, "Sparse representation of monogenic signal: With application to target recognition in SAR images," *IEEE GRSL*, Vol. 21, No. 8, 952–956, 2014.
16. Clemente, C., et al., "Pseudo-Zernike based multi-pass automatic target recognition from multi-channel SAR," *IET RSN*, Vol. 9, No. 4, 457–466, 2015.
17. Mishra, A. K. and B. Mulgrew, "Bistatic SAR ATR using PCA-based features," *Automatic Target Recognition XVI*, Vol. 6234, International Society for Optics and Photonics, 2006.
18. Ash, J. N., "Joint imaging and change detection for robust exploitation in interrupted SAR environments," *Algorithms for Synthetic Aperture Radar Imagery XX*, Vol. 8746, 87460J, International Society for Optics and Photonics, 2013.
19. Zhang, Y. D., L. Wu, and G. Wei, "A new classifier for polarimetric SAR images," *Progress In Electromagnetics Research*, Vol. 94, 83–104, 2009.
20. Zhai, Y., J. Li, J. Gan, and Z. Ying, "A multi-scale local phase quantization plus biomimetic pattern recognition method for SAR automatic target recognition," *Progress In Electromagnetics Research*, Vol. 135, 105–122, 2013.

21. Mishra, B. and J. Susaki, "Coupling of thresholding and region growing algorithm for change detection in SAR images," *Progress In Electromagnetics Research*, Vol. 143, 519–544, 2013.
22. Gao, G., X. Qin, and S. Zhou, "Modeling SAR images based on a generalized gamma distribution for texture component," *Progress In Electromagnetics Research*, Vol. 137, 669–685, 2013.
23. Cheng, J., G. Gao, W. Ding, X. Ku, and J. Sun, "An improved scheme for parameter estimation of G° distribution model in high-resolution SAR images," *Progress In Electromagnetics Research*, Vol. 134, 23–46, 2013.
24. Ni, W. P., W. D. Yan, J. Z. Wu, et al., "Moment feature analysis and multi-threshold segmentation of MSTAR image," *JOIG*, Vol. 18, No. 10, 2018.
25. Fu, F. C., "SAR target recognition method based on target region matching," *EO&C*, Vol. 4, 2018.
26. Ding, J., B. Chen, H. Liu, et al., "Convolutional neural network with data amplification for SAR target recognition," *IEEE*, Vol. 13, No. 3, 364–368, 2016.
27. Chen, S., H. Wang, F. Xu, et al., "Target classification using the deep convolutional networks for SAR images," *IEEE TGRS*, Vol. 54, No. 8, 4806–4817, 2016.
28. Zhao, W. and S. Du, "Spectral-spatial feature extraction for hyperspectral image classification: A dimension reduction and deep learning approach," *IEEE TGRS*, Vol. 54, No. 8, 4544–4554, 2016.
29. Marmanis, D., M. Datcu, T. Esch, et al., "Deep learning earth observation classification using ImageNet pertained networks," *IEEE GRSL*, Vol. 13, No. 1, 105–109, 2016.
30. AbdAlmageed, W., Y. Wu, S. Rawls, et al., "Face recognition using deep multi-pose representations," *2016 IEEE Winter Conference on Applications of Computer Vision (WACV)*, 1–9, IEEE, 2016.
31. Morgan, D. A. E., "Deep convolutional neural networks for ATR from SAR imagery," *Algorithms for Synthetic Aperture Radar Imagery XXII*, Vol. 9475, 94750F, International Society for Optics and Photonics, 2015.
32. Profeta, A., A. Rodriguez, and H. S. Clouse, "Convolutional neural networks for synthetic aperture radar classification," *Algorithms for Synthetic Aperture Radar Imagery XXIII*, 9843–98430M, International Society for Optics and Photonics, 2016.
33. Wilmanski, M., C. Kreucher, and J. Lauer, "Modern approaches in deep learning for SAR ATR," *Algorithms for Synthetic Aperture Radar Imagery XXIII*. International Society for Optics and Photonics, 9843–98430N, 2016.
34. Ødegaard, N., A. O. Knapskog, C. Cochin, et al., "Classification of ships using real and simulated data in a convolutional neural network," *2016 IEEE Radar Conference*, 1–6, IEEE, 2016.
35. Liu, C., C. W. Qu, et al., "Target classification of SAR images based on convolution neural network migration learning," *Modern Radar*, Vol. 3, 2018.
36. Krizhevsky, A., I. Sutskever, and G. E. Hinton, "ImageNet classification with deep convolutional neural networks," *International Conference on Neural Information Processing Systems*, Curran Associates Inc., 2012.
37. Lecun, Y. L., et al., "Gradient-based learning applied to document recognition," *Proceedings of the IEEE*, Vol. 86, No. 11, 2278–2324. 1998.
38. He, K. M., et al., "Deep residual learning for image recognition," *2016 IEEE Conference on Computer Vision and Pattern Recognition (CVPR)*, 2016.
39. Qi, H. J., Y. H. Wang, J. Ding, et al., "SAR target recognition based on Multi-information dictionary learning and sparse representation," *J. Syst. Eng. Electron.*, Vol. 37, No. 6, 1280–1287, 2015.
40. Wu, T., et al., "Study on SAR target recognition based on Support Vector Machine," *IEEE Conference on Synthetic Aperture Radar, Asian-Pacific*. 856–859, 2010.
41. Zhai, Y. K., J. Li, J. Y. Gan, et al., "A multi-scale local phase quantization plus biomimetic pattern recognition method for SAR automatic target recognition," *Progress In Electromagnetics Research*, Vol. 135, No. 1, 105–122, 2013.
42. Wang, L., F. Zhang, W. Li, et al., "A method of SAR target recognition based on gabor filter and local texture feature extraction," *JOR*, Vol. 4, No. 6, 658–665, 2015.

43. Zhang, H., N. M. Nasrabadi, Y. Zhang, et al., "Multi-view automatic target recognition using joint sparse representation," *IEEE Transactions on Aerospace and Electronic Systems*, Vol. 48, No. 3, 2481–2497, 2012.
44. Tian, Z. Z., R. H. Zhan, J. M. Hu, et al., "SAR ATR based on convolutional neural network," *Journal of Radars*, Vol. 5, No. 3, 320–325, 2016.
45. Sun, Y., Z. Liu, S. Todorovic, et al., "Adaptive boosting for SAR automatic target recognition," *IEEE Transactions on Aerospace and Electronic Systems*, Vol. 43, No. 1, 112–125, 2007.
46. Liu, K. P., Z. L. Ying, and Y. K. Zhai, "SAR image target recognition based on unsupervised k-means feature and data amplification," *JOSP*, Vol. 33, No. 3, 456–458, 2017 (in Chinese).